Whispering Gallery Modes in a Dielectric Resonator: Characterization at Millimeter Wavelength

Giuseppe Annino, Mario Cassettari, Iginio Longo, and Massimo Martinelli

***Abstract*—Applications of whispering-gallery-mode (WGM) dielectric resonators in the millimeter and submillimeter frequency range are discussed. A summary of the main peculiarities of these resonators is given, and a method to obtain approximate analytical expressions of electromagnetic field components is developed. Problems connected with the excitation by far infrared (FIR) laser radiation are examined. The analysis of electromagnetic propagation in different structures drives the best choice for the transmission line (metallic and dielectric waveguides), and the same theoretical analysis allows to face the basic problem of optimizing the matching between transmission-line and WG resonators; the role in this application of dielectric waveguides with variable diameter is discussed. All of the predictions are obtained in a unified theoretical picture. The experimental characterization of a WG resonator at 240 GHz involved the measurement of the effectiveness of the coupling between the transmission line and the resonator, the determination of the merit factor and free spectral range for the different resonance families in different resonators. Accurate measurements were carried out to acquire knowledge of the field distribution in both axial and radial directions; to this purpose, dielectric antennas with high directivity were used to sense the field intensities for different resonance modes. The good agreement between the experimental results and the theoretical predictions is carefully discussed.**

***Index Terms*—Dielectric resonators, far infrared (FIR) radiation, whispering gallery modes.**

I. Introduction

THE SEARCH for an efficient and handy resonator in the millimeter and submillimeter wavelength range is acquiring more and more importance as far as the number of its applications is growing. The need for integrated components or supercomponents in this spectral range for applications in the field of communications gives impulsion to this search [1]–[5]; spectroscopy and other research applications from millimeter up to optical wavelengths, however, are not a negligible part of this effort [6]–[11]. Main devices exploiting resonators include power combiners, frequency multiplexers and demultiplexers, filters, and cavity-tuned oscillators. In many cases, the use of resonators with high merit factor Q guarantees the building up of radiation sources with spectral noise characteristics that are appealing for spectroscopy and metrology applications.

The use of *quasi-optical* propagation techniques becomes mandatory when frequency increases and the use of standard TE or TM metallic cavities shows some drawbacks. On the other hand, Fabry–Perot resonators, when efficiently coupled at wavelengths of about 1 mm, show low Q-factors [12]. Commercial dielectric resonators operating in TE and TM modes are useful for lower frequencies, but become exceedingly small and their Q-factors are strongly reduced when the wavelengths approach the far infrared (FIR) range [13]. On the contrary, dielectric resonators operating in hybrid modes known as whispering gallery modes (WGM's), investigated originally by Vedrenne and Arnaud [14], avoid many of the above constraints and can be usefully employed in the submillimeter range also [15]. The most important characteristics of these resonators for applications are the not necessarily very small size and the high Q achieved depending on the material used. Another interesting feature of these resonators is the availability of a multiplicity of resonances (not harmonically related), observable in an ultrawideband range from the microwave to the visible radiation. Moreover, their *finesse* in this spectral range is still remarkably high. A research field in which the availability of resonators with suitable characteristics is a crucial point is the electron paramagnetic resonance (EPR) spectroscopy performed at high magnetic field ($>$10 T) [16]. In this application, the radiation produced by the source is transmitted to a resonator containing the sample embedded in an intense magnetic field. The radiation after the interaction with the sample inserted in the resonator carries the information about the absorption of energy at magnetic resonance and can be used to characterize the sample spectrally. This information is recovered by a detector and then processed. The resonance condition is obtained when the value of magnetic field H_0 fulfils the condition

$$\omega = \gamma H_0 \tag{1}$$

where ω is the angular frequency of the source and γ is the magnetogyric constant that is connected with magnetic characteristics of the system studied; typical values are $\gamma/2\pi = 2.8$ MHz/Gauss. With the intensities of magnetic field used for this new spectroscopy ($>$10 T), the radiation frequency grows up to the submillimeter range.

The radiation source could be either a solid-state source (Gunn or IMPATT) or a molecular FIR laser. The first one is a handy apparatus that has capabilities for electronic frequency tuning but limited working frequency ranges and very low emitted power at increasing frequencies; on the contrary, FIR lasers are demanding apparatus that have very poor instantaneous frequency tunability. However, FIR lasers have a practically unlimited emission spectral range (up to some terahertz) in many bands selected according to the molecular system and, in general, the emitted power increases with

Manuscript received February 11, 1997; revised July 18, 1997.

G. Annino was with the Istituto di Fisica Atomica e Molecolare, C.N.R., 56127 Pisa, Italy. He is now with the Scuola Normale Superiore and INFM, 56126 Pisa, Italy.

M. Cassettari, I. Longo, and M. Martinelli are with the Istituto di Fisica Atomica e Molecolare, C.N.R., 56127 Pisa, Italy.

Publisher Item Identifier S 0018-9480(97)08020-4.

increasing frequency. Finally, a careful setup of the laser guarantees very good spectral characteristics of the emitted radiation [17]. The experiments here described were performed with an FIR laser operating at about 240 GHz.

The resonator is an essential component in order to increase the density of electromagnetic energy at the sample and to enhance the measurement sensitivity [18]. The different characteristics of disc-shaped dielectric resonators working with WGM's seem appealing for high-field EPR applications. Two main problems involve the transmission of radiation field to the resonator:

1) the synchronization of the resonance frequency of the WGM resonator with the frequency of radiation feeding the resonator itself;
2) the optimization of energy transfer from the source to the resonator.

The first problem arises from the scarce tunability of FIR laser sources; also in the case of molecular lines shifted by electric fields, the tuning range is not greater than a few tens of MHz [17]. A possibility is to change the resonance frequency of the resonator.

The second aspect concerns the efficient transmission of radiation from the source to the resonator containing the sample—since the magnetic field is generated by a large superconducting magnet, the radiation has to be transmitted on a few meters. A satisfactory solution for this purpose is given by the use of oversized conducting waveguides that guarantee very low attenuation [19]. When the radiation reaches the resonator, particular care has to be taken in the coupling with the resonator in order to optimize the transfer of power to the resonator itself without affecting its merit factor and to enable the control of the excitation of the different resonance modes. The plan of this paper is the following. In Section II we give a summary of the main peculiarities of WGM's in dielectric disc resonators, developing a method to give approximate analytical expressions of e.m. field components. In Section III we discuss the methods for transferring the electromagnetic energy in the millimetric and submillimetric range to the WGM resonators and for tuning the resonators across the resonance. In Section IV we describe the experimental apparatus; in Section V we show the experimental characterization of different resonance modes, making the comparison with theoretical predictions.

II. Whispering Gallery Modes in a Planar Circular Dielectric Resonator

In an infinite circular cylindrical dielectric structure with constants ε_1, μ_1 plunged in a medium with constants ε_2, μ_2, the elementary solution of the wave equation for the longitudinal components of fields has, in terms of cylindrical coordinates, the general expression [20]

$$A_{zn}(\rho, \varphi, z, t) = C(n) Z_n(\beta\rho) e^{in\varphi - ihz + i\omega t}. \tag{2}$$

In (2), that holds true in all the space inside and outside the cylinder; the $Z_n(\beta\rho)$ are the solutions of the Bessel equation. Inside the cylinder such solutions are the first kind Bessel functions J_n with argument $\beta_1\rho$ where β_1 is defined by $\beta_1^2 = \varepsilon_1\mu_1\omega^2 - h^2 = k_1^2 - h^2, h$ being the axial propagation constant. Outside the cylinder, the solutions are the Hankel functions $H_n^{(2)}$ with argument $\beta_2\rho$ where β_2 is defined by $\beta_2^2 = \varepsilon_2\mu_2\omega^2 - h^2 = k_2^2 - h^2$. All of the other components of fields can be obtained by the longitudinal components [21]. The coefficients giving the amplitude of different field components and related h values are unknown quantities connected by the boundary conditions at the surface of the cylinder. These quantities are obtained by solving the characteristic equation, which is for nonmagnetic materials $(\mu_1 = \mu_2 = \mu_0)$ [20]

$$\left[\frac{J_n'(u)}{uJ_n(u)} - \frac{H_n^{(2)'}(v)}{vH_n^{(2)}(v)}\right] \cdot \left[\frac{\varepsilon_1 J_n'(u)}{uJ_n(u)} - \frac{\varepsilon_2 H_n^{(2)'}(v)}{vH_n^{(2)}(v)}\right] = \frac{n^2h^2}{\omega^2\mu_0\varepsilon_0}\left(\frac{1}{u^2} - \frac{1}{v^2}\right)^2 \tag{3}$$

where $u = \beta_1 a$ and $v = \beta_2 a$ are the arguments of Bessel and Hankel functions, respectively, $\boldsymbol{a}$ being the radius of the cylinder. Equation (3) is a transcendental equation giving the eigenvalues for h. The eigenfunctions associated to these eigenvalues are the modes of the electromagnetic waves propagating in the considered structure (natural modes) [21].

When the cylinder is used as a waveguide, the analysis of undamped modes corresponding to a real axial propagation constant h is particularly interesting. In this case the boundary conditions at cylinder surface imply the condition

$$k_1^2 > h^2 > k_2^2 \tag{4}$$

provided that $\varepsilon_1 > \varepsilon_2$ [22]. It must be pointed out [23] that the solution of the Bessel equation in that part of space inside the cylinder is oscillating for $\rho > \rho_c$ and monotonically decreasing for $\rho < \rho_c$; the surface

$$\rho_c = \frac{|n|}{\beta_1} = \frac{|n|}{\sqrt{k_1^2 - h^2}} \tag{5}$$

is defined modal caustic. The radiation in the cylinder actually propagates confined between the caustic and the rim. Particular solutions of (3) correspond to the WGM's for which the caustic is very close to the surface of the cylinder; such modes propagate spirally near the boundary of the cylinder [24].

A resonator oscillating with the modes solution of (3) is obtained by reducing the infinite cylinder to a cross section with finite length. This length must be relatively small in order to separate the different resonance modes [15]. The propagation constant h becomes complex and for reduced axial dimension of the resonator the condition $\mathrm{Re}\{h\} < k_2$ can be assumed. The behavior of the electromagnetic waves in this case is meaningfully obtained by an expansion of the modes of the cylinder in plane waves. From the relation $(\beta_1^2/k_1^2) + (h^2/k_1^2) = 1$ it can be introduced the angle $\Theta = \alpha + i\delta$, fulfilling the conditions

$$\beta_1 = k_1 \sin\Theta \qquad h = k_1 \cos\Theta \tag{6}$$

where

$$\begin{aligned} \sin\Theta &= \sin\alpha \cdot \cosh(\delta) + i\cos\alpha \cdot \sinh(\delta) \\ \cos\Theta &= \cos\alpha \cdot \cosh(\delta) - i\sin\alpha \cdot \sinh(\delta). \end{aligned} \tag{7}$$

It can be useful to introduce the integral representation of Bessel functions [21]

$$2\pi J_n(\eta) = \int_{-\pi}^{\pi} e^{i\eta\cos\phi} e^{in(\phi-(\pi/2))}\, d\phi \tag{8}$$

which is effective also for complex argument [20]; the insertion of expressions (6) in (8) gives, by taking into account the definitions (7)

$$\begin{aligned} &2\pi J_n(\beta_1\rho)e^{i(n\varphi-hz+\omega t)} \\ &\quad = \int_{-\pi}^{\pi} e^{i\{-k_1[x\sin\Theta\cos\phi+y\sin\Theta\sin\phi+z\cos\Theta]+\omega t\}} \\ &\qquad \cdot e^{in(\phi+(\pi/2))}\, d\phi. \end{aligned} \tag{9}$$

The exponential term containing the complex angles can be separated in terms related to the propagation and in terms related to the damping

$$\begin{aligned} &e^{-ik_1[x\sin\Theta\cos\phi+y\sin\Theta\sin\phi+z\cos\Theta]} \\ &\quad = e^{-ik_1[x\sin\alpha\cosh\delta\cos\phi+y\sin\alpha\cosh\delta\sin\phi+z\cos\alpha\cosh\delta]} \\ &\qquad \times e^{-k_1[x\sin\alpha_d\sinh\delta\cos\phi+y\sin\alpha_d\sinh\delta\sin\phi+z\cos\alpha_d\sinh\delta]} \end{aligned} \tag{10}$$

where $\alpha_d = \alpha - \pi/2$. Equations (9) and (10) show that the considered mode can be expressed as an expansion in inhomogeneous plane waves that propagate in a direction forming an angle α with the axis z of the cylinder, having the propagation constant $k_1\cosh(\delta) \geq k_1$ and damped along the perpendicular direction corresponding to the angle α_d with a propagation constant $k_1\sinh(\delta)$.

Since the attention is concentrated upon the weakly damped modes for which $\cosh(\delta) \approx 1$ and $\sinh(\delta) \approx \delta$, the expressions (7) can be rewritten as

$$\sin\Theta \approx \sin\alpha + i\delta\cos\alpha \qquad \cos\Theta \approx \cos\alpha - i\delta\sin\alpha.$$

Consequently, $\mathrm{Re}\{h\} \approx k_1\cos\alpha$ and $\mathrm{Re}\{\beta_1\} \approx k_1\sin\alpha$. This implies that the mode is a superposition of plane waves with wavenumber k_1 that propagate in a direction forming an angle α with the axis of the cylinder. The hypothesis $\mathrm{Re}\{h\} < k_2$ now implies

$$\cos\alpha < \frac{k_2}{k_1} = \cos\left[\frac{\pi}{2} - \Theta_e\right]$$

where

$$\Theta_e = \sin^{-1}\left(\frac{\varepsilon_2}{\varepsilon_1}\right)^{1/2}. \tag{11}$$

Consequently, $\alpha > [(\pi/2) - \Theta_e]$; the damped mode, according to this model, corresponds to the radiation propagating with angles α for which energy is irradiated outside the cylinder.

When $\mathrm{Re}\{h\} \approx 0$, the angle α assumes the value $\alpha = \pi/2$; the propagation then occurs in a plane perpendicular to the axis of the cylinder. The damping will be negligible only for that radiation having an angle of incidence at the surface of the cylinder larger than the angle Θ_e. This occurs, for instance, in the case of WGM's that are confined near the rim of the cylinder.

In order to describe the propagation of WGM's in the cylinder, it is useful to exploit the geometric optics representation.

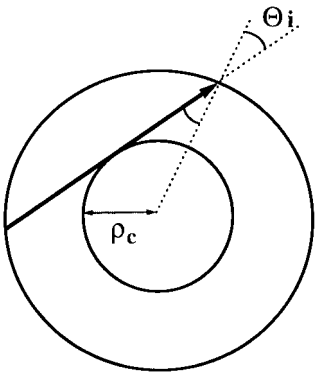

Fig. 1. Cross section of the dielectric cylinder with the optical ray representing the radiation propagating tangentially to the caustic.

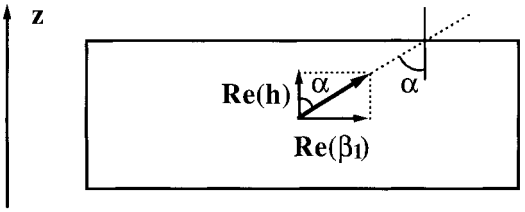

Fig. 2. Schematic representation of propagation inside a finite cylinder.

Within this representation the propagation occurs tangentially to the caustic (Fig. 1). The angle of incidence Θ_i in terms of the modal caustic definition is written

$$\Theta_i = \sin^{-1}\left(\frac{\rho_c}{a}\right) = \sin^{-1}\left(\frac{n}{\beta_1 a}\right). \tag{12}$$

Equation (12) shows that when the modal index n increases (and the ray of caustic increases, too) the condition $\Theta_i > \Theta_e$ is well fulfilled and the losses for the WGM's decrease [23].

When the cylinder has a finite axial dimension, the requirement of weak losses for the considered mode implies the condition of total reflection also on the bases of the cylinder. Fig. 2 shows schematically the propagation inside the finite cylinder to be used as resonator. Total reflection occurs when $\sin\alpha > (\varepsilon_2/\varepsilon_1)^{1/2}$ and the condition for the axial propagation becomes, under the weak loss limit

$$\mathrm{Re}\{h\} \leq \left(1 - \frac{\varepsilon_2}{\varepsilon_1}\right)^{1/2} k_1.$$

When a planar WG resonator has to be used it is particularly important to study the distribution of e.m. fields in WGM's with axial propagation constant $\mathrm{Re}\{h\} \approx 0$ [14]. In presence of small losses also $\mathrm{Im}\{h\} \approx 0$, then $h \approx 0$. The expression of different components of fields can be obtained starting from (3).

Under the hypothesis $h \to 0$ the quantity $(1/u^2) - (1/v^2) \to (1/a^2)((1/k_1^2) - (1/k_2^2)) \neq 0$ then the term on the right in (3) vanishes as h^2. One of the following conditions must consequently hold true:

$$\frac{J_n'(u)}{uJ_n(u)} - \frac{H_n^{(2)'}(v)}{vH_n^{(2)}(v)} \to 0(h^2) \tag{13a}$$

$$\frac{\varepsilon_1 J_n'(u)}{uJ_n(u)} - \frac{\varepsilon_2 H_n^{(2)'}(v)}{vH_n^{(2)}(v)} \to 0(h^2) \tag{13b}$$

provided that common roots do not exist.

Like the procedure used for evaluation of natural modes in the dielectric cylinder [21], it is useful to introduce the parameter $\alpha_{n,m}$ defined by

$$\alpha_{n,m} = \frac{\omega\mu_0 b_{n,m}}{i h_{n,m} a_{n,m}} \tag{14}$$

where the quantities a, b are, for each mode, the coefficients of the expansion in terms of Bessel functions giving the longitudinal components of the electric and magnetic fields, respectively. The index m is an integer number that accounts for the different solutions of (3) for a fixed n value. The parameter $\alpha_{n,m}$ can be expressed in terms of roots of the characteristic equation by using the boundary conditions [21]

$$\alpha_{n,m} = \frac{n\left(\frac{1}{u^2} - \frac{1}{v^2}\right)}{\frac{J_n'(u)}{uJ_n(u)} - \frac{H_n^{(2)'}(v)}{vH_n^{(2)}(v)}} = \frac{\frac{\varepsilon_1 J_n'(u)}{uJ_n(u)} - \frac{\varepsilon_2 H_n^{(2)'}(v)}{vH_n^{(2)}(v)}}{n\left(\frac{\varepsilon_1}{u^2} - \frac{\varepsilon_2}{v^2}\right)} \tag{15}$$

where the indexes n, m in the different quantities were omitted for the sake of simplicity. By introducing the condition (13a) in the expression (15), it is possible to argue that $a_{n,m} \to 0$ as h for each n, m. The expressions for the different components of fields for the WGM's are then calculated from the general equations of fields in a cylinder [20]. For $\rho \le a$ the fields are

$$\begin{aligned}
E_z &\approx 0 + o(h)\\
H_z &\approx b_{n,m} J_n(k_1\rho)\\
E_\rho &\approx b_{n,m}\frac{\omega\mu_0 n}{k_1^2\rho} J_n(k_1\rho) + o(h^2)\\
&\approx \pm b_{n,m}\frac{\omega\mu_0}{k_1} J_n(k_1\rho)\\
H_\rho &\approx 0 + o(h)\\
E_\varphi &\approx i b_{n,m}\frac{\omega\mu_0}{k_1} J_n'(k_1\rho) + o(h^2)\\
&\approx i b_{n,m}\frac{\omega\mu_0}{k_1} J_n'(k_1\rho)\\
H_\varphi &\approx 0 + o(h)
\end{aligned} \tag{16}$$

where it was used the approximation $\beta_1 a \approx \beta_1\rho \approx |n|$, valid for WGM's, in the limit $h \to 0$. The same procedure gives analogous expressions for the components of the fields for $\rho > a$. In all of the expressions (16), the factor $e^{in\varphi + i\omega t}$ is omitted. The mode considered is a TE mode that, in general, is named WGE mode.

If, on the contrary, the condition (13b) is introduced in (15), some algebraic manipulations give in the limit $h \to 0$

$$\alpha_{n,m} = \frac{n}{a^2}\left(\frac{1}{k_1^2} - \frac{1}{k_2^2}\right)\left[\frac{J_n'(u)}{uJ_n(u)} - \frac{H_n^{(2)'}(v)}{vH_n^{(2)}(v)}\right]^{-1}$$

that is, α_{nm} has a finite value; by considering (14), since $a_{n,m}$ has a finite value, $b_{n,m} \to 0$ as h for each n, m. Following the same procedure as previously, it is possible also in this case to write the components of fields. For $\rho \le a$

$$\begin{aligned}
E_z &\approx a_{n,m} J_n(k_1\rho)\\
H_z &\approx 0 + o(h)\\
E_\rho &\approx 0 + o(h)\\
H_\rho &\approx -a_{n,m}\frac{\omega\varepsilon_1 n}{k_1^2\rho} J_n(k_1\rho) + o(h^2)\\
&\approx \mp a_{n,m}\frac{\omega\varepsilon_1}{k_1} J_n(k_1\rho)\\
E_\varphi &\approx 0 + o(h)\\
H_\varphi &\approx -i a_{n,m}\frac{\omega\varepsilon_1}{k_1} J_n'(k_1\rho) + o(h^2)\\
&\approx -i a_{n,m}\frac{\omega\varepsilon_1}{k_1} J_n'(k_1\rho).
\end{aligned} \tag{17}$$

For $\rho > a$ the fields show the same dominant components. Also in (17), the factor $e^{in\varphi + i\omega t}$ is omitted. The mode in this case is a TM and is named WGH mode.

The modes represented in (16) and (17) are the solutions of the wave equations corresponding to weak axial propagation that give an approximate picture of e.m. fields in a plane with $z =$ constant in disc-shaped dielectric resonators. Such results can be compared to the shape of fields obtained for this type of resonator with a numeric solution of Maxwell equations [15].

By summarizing, the WGE or WGH resonance modes in a planar dielectric structure are characterized by the modal indexes n, m, l. The index n indicates the number of complete periods of wave during a whole turn around the resonator; n coincides with the order of the Bessel function defining the longitudinal field. An unambiguous definition for m is the number of nodes of the energy flux encountered along the radius. The index l is connected to the behavior of fields in the axial direction; the approximations introduced in calculating the WGE and WGH modes do not allow an exact determination of this index that is related to the number of nodes of the energy flux along the axis of the resonator. A reasonable evaluation can be obtained by supposing that axial propagation is like that in a dielectric plane plate; in this case, the fundamental solutions are oscillating with defined parity inside the plate ($\cos\{hz\}$ and $\sin\{hz\}$) and decreasing exponentially outside the plate [21].

III. Coupling of the Radiation to WG Dielectric Resonators

It can be demonstrated that the matching between modes of two different systems in which electromagnetic waves are propagating (in this case the waveguide and the WG resonator) is maximum when the propagation constants of the two modes coincide; that is, when the phase velocity of the electromagnetic waves is the same [25]. The WGM's with azimuthal index n in a planar circular dielectric resonator with radius a, within the limit of negligible axial propagation, have the phase of fields characterized by the factor $e^{in\varphi + i\omega t}$ (16), (17); the angular phase velocity associated is

$$\frac{\partial\varphi}{\partial t} = -\frac{\omega}{n}.$$

Within the approximation that the wave circulates only very close to the rim of the planar resonator, which is well fulfilled

particularly when the considered modes have $m = 0$, the constant phase planes travel with a tangential velocity

$$v_\varphi = -\frac{\omega a}{n} = \frac{k_1 a}{n\sqrt{\varepsilon\mu_0}} \approx \mp\frac{c}{\sqrt{\varepsilon_r}} \tag{18}$$

where the approximation $\rho_c = a$, valid for WG modes, was assumed for the caustic (5); here c is the light velocity in the vacuum and ε_r is the relative dielectric permittivity of the resonator. Equation (18) says that the phase velocity for WGM's in the resonator made of a given material has the same value as for a plane wave freely propagating in this material. Dielectric cylindrical waveguides will be considered for transmission since they do not bind completely the radiation. An electromagnetic wave represented by the general expression (2) and propagating in a dielectric cylinder with radius r has the phase velocity along the axis of the guide given by $v_\varphi = \omega/h$. It must be pointed out that the wave is present in general in the whole space inside and outside the cylinder; for undamped modes, h becomes real and fulfills the condition (4). The phase velocity must then fulfill the condition $v_{\varphi 1} < v_\varphi < v_{\varphi 2}$.

The limit conditions $h \to k_1$ and $h \to k_2$ in (4) correspond to the *far from cutoff* and *cutoff* conditions, respectively [21]. Restricting the discussion of Section II to the case of a real angle of propagation, it gets out that the angle $\alpha \to 0$ when $h \to k_1$; in this limit, the plane waves propagate parallel to the axis of cylindrical structure and the whole energy is confined inside the guide. When $h \to k_2$, starting from $h > k_2, \beta_1^2/k_1^2 = 1 - (\varepsilon_2/\varepsilon_1)$ and $\sin\alpha = \sqrt{1 - \sin^2\Theta_e}$; the angle of propagation tends to the limit angle.

The extent of the evanescent field and its energy outside the guide increases when Θ_i, the angle of incidence of the plane waves at the surface of the cylinder, decreases toward Θ_e. The refracted wave appears when $\Theta_i < \Theta_e$; in this condition h becomes a complex quantity and the mode is damped due to the wave irradiated outside the cylinder. For the fundamental mode HE_{11} the two limit conditions are fulfilled when $r \to \infty$ and $r \to 0$, respectively. When r is changed, the theorem of implicit functions, applied to (3), guarantees the continuous variation of h between the limit values corresponding to the *far from cutoff* and *cutoff* conditions. The change of r implies then the continuous variation of the phase velocity of the propagating wave between the value characteristic of the medium with which the waveguide is formed and the one of the medium surrounding the guide. It will be always possible to obtain in the range between the *far from cutoff* and the *cutoff* conditions a phase velocity like that of (18), provided that the permittivity of the dielectric guide is larger than that of the resonator. Fig. 3 shows the trend of the phase velocity for the mode HE_{11} as a function of r for different values of the relative permittivity of the material forming the guide, obtained by solving numerically (3). It is then always possible to obtain a good matching between a dielectric waveguide and a dielectric WGM resonator either by a proper choice of the waveguide diameter or by using a cone-shaped waveguide coupler properly positioned near the resonator. The coupling will be obtained overlaying the evanescent field of the resonator with the evanescent field outside the cylindrical

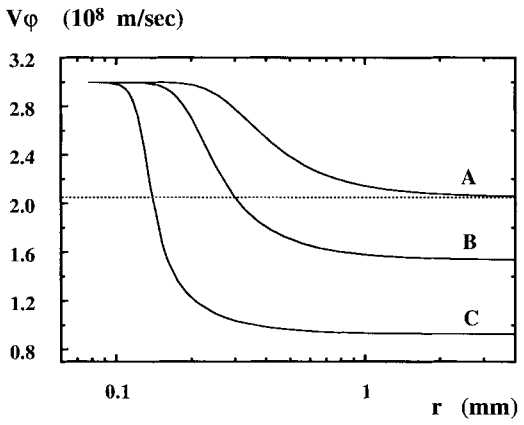

Fig. 3. Phase velocity of the HE_{11} mode as a function of the radius of the dielectric waveguide for different values of the relative permittivity ε_1. Curve A: $\varepsilon_1 = 2.1345$; curve B: $\varepsilon_1 = 3.81$; curve C: $\varepsilon_1 = 10.5$. The straight dotted line, traced for reference, indicates the phase velocity in a polyethylene resonator.

waveguide. When a tapered waveguide is used, the matching is obtained by moving the resonator along the direction of the axis of the tapered waveguide up to the position where the respective phase velocities coincide.

The requirement of an effective coupling implies, on the other hand, that a remarkable field intensity is present in the zone of interaction between the two devices [25]. The excess of losses due to the irradiation must be so avoided by making the variation of the radius of the coupler to occur over distances much greater than the wavelength. Furthermore, the choice of dielectric properties of materials must imply that the condition of identity of phase velocities is fulfilled where the diameter of the tapered guide approaches the value of the wavelength in the medium; in this point, the evanescent field intensity around the guide reaches approximately its maximum value.

IV. The Apparatus and Experimental Methods

The radiation source used during experiments was an FIR laser (Edinburgh Instruments model 295) pumped by a CO_2 laser (Edinburgh Instruments model PL5); the active medium was methyl iodide CH_3I, giving a line at 239.1 GHz. The power obtained from the source at this frequency was about 0.6 mW. The emission of the FIR laser took place through a window with 13-mm diameter; the transmission of the power was assured with very small losses [19] by a brass cylindrical waveguide with the same diameter as the window. The metallic waveguide was terminated by a tapered fused quartz waveguide, allowing the coupling with the dielectric disc resonator, as discussed in the previous section. The resonators used for measurements were 0.8-mm-thick discs of 30-mm diameter, made out with high-density polyethylene. This choice was suggested both by the values of the permittivity of the polyethylene and by its extreme ease in the mechanical processing. The position of the resonator was kept fixed near the point of the tapered guide having a diameter of about 0.6 mm; in this configuration the coupling was satisfactory. This is consistent with theoretical predictions of Fig. 3 where the dotted straight line, representing the phase velocity in the polyethylene resonator, crosses the curve

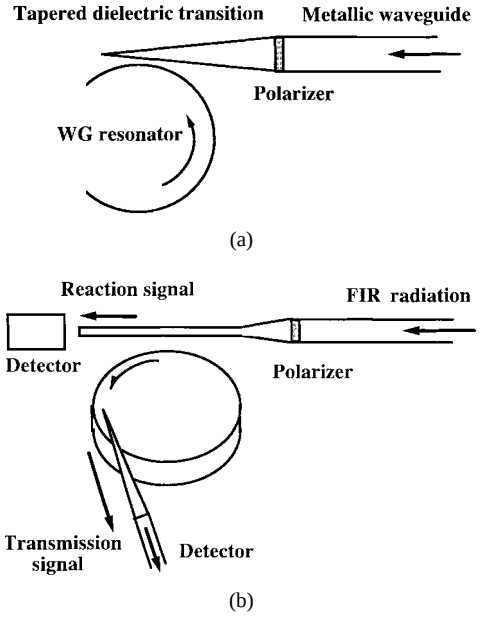

Fig. 4. Schemes for coupling radiation to the resonator. (a) Tapered dielectric transition. (b) Reaction scheme with constant radius coupling. The pickup antenna is also indicated.

calculated for the fused quartz, just near the value of the radius $r = 0.3$ mm.

In order to determine experimentally the spatial distribution of fields for the different WGM's and compare it with the approximate predictions of (16) and (17), one needs a probe working like an antenna with a proper directivity. If a dielectric rod with finite length is used as an antenna, its emission characteristics can be obtained by a procedure based on the Huygens principle and on optical geometry [26]. This analysis suggests that the best directivity is obtained with a tapered shape; in particular for the fundamental mode HE_{11}, this occurs when the diameter of the guide tends to zero and the propagation reaches the cutoff condition. The antenna used in measurements was a tapered rod made with fused quartz equipped with a very sharp tip; a better spatial resolution is obtained when the permittivity of the antenna is much larger than that of the resonator since in this case the matching of the phase velocities between the two devices, useful for the coupling of radiation, occurs only just near the tip (Fig. 3). The radiation drawn by the antenna was transmitted by a properly shaped metal waveguide to a Golay detector. A laser beam chopper working at 17 Hz was introduced, allowing the signal phase sensitive detection.

It must be pointed out that the polarization of the wave transmitted by the waveguide to the resonator is very important in order to excite selectively each requested mode. The part of the transmission line made with the metallic waveguide propagates with lowest attenuation the mode TE_{01} that does not show a linear polarization [19]; a wire polarizer was placed at the end of the metallic waveguide where a tapered dielectric rod is inserted [Fig. 4(a)]. A beam polarization better than 90% and negligible attenuation were obtained.

The tuning of the resonance frequency of the resonator was obtained efficiently by using a conducting circular plate placed parallel to the disc at a variable distance. Numerical calculations [15] predicted this tuning effect and demonstrated that the structure of fields is not modified significantly. This effect can be described by a phenomenological equation by taking into account the exponential decay of the evanescent field near the surface of interest. The variation $\Delta\nu$ of the resonance frequency when the plane of the conductor is moved of a quantity Δz toward the resonator is given by

$$\Delta\nu = A_{nml}(e^{B_{nml}\Delta z} - 1) \tag{19a}$$

where the constant terms A and B account for the different effects produced by the conductor for different resonance modes. Since the quantity experimentally determined is the relative displacement Δz, (23a) can be usefully rewritten as

$$\Delta z = B_{nml}^{-1} \ln\left(A_{nml}^{-1}\Delta\nu + 1\right). \tag{19b}$$

The shape and size of the tuning plate must be optimized according to the mode to be studied; in general, it will have a ring shape with size consistent with the predicted spatial mode distribution. Experiments were carried out tuning the resonances with a brass ring with external diameter of 30 mm and internal diameter of 27.5 mm. A micrometer screw with resolution of 10^{-2} mm acted on the tuner at different distances along the axis of the resonator. The same type of micrometer screw was used to drive the dielectric antenna across the resonator surface to study the different parameters of interest.

Main experimental procedures included:

1) analysis of the coupling procedure, measurement of the effectiveness of the coupling;
2) methods for determining Q merit factor of different resonances and the free spectral range;
3) spatial distribution of field intensities in the resonator for the different resonances and determination of the different modal indexes for each resonance.

For point 1), a better control of the different parameters of the coupling method was obtained by measuring simultaneously the reaction and transmission signals [Fig. 4(b)]. After the determination of the best value for the diameter of excitation guide according to the procedure discussed in the previous section, the coupling condition was controlled by changing the distance between the excitation guide and the resonator. The simultaneous observation of the reaction and transmission signals allowed the evaluation of spurious effects in the transmission line induced by the interaction line-resonator. The reaction signal was measured by coupling the end of the waveguide to a detector. For the transmission signal, a tapered dielectric antenna drew the wave at the surface of resonator in a fixed position selected for each resonance; the wave was then coupled to a second detector.

Point 2) implies the determination of the quality of the structure used as a resonator and the distribution of different resonance families. A proper choice of size and quality of the shape of the resonator in fact makes the Q-factor depending mainly on the intrinsic losses of the material and determines the free spectral range between each couple of resonances. During these measurements the coupling structure was kept in fixed condition and the wave was drawn by the dielectric

antenna placed at the surface of the resonator where the observed signal was maximum. The shape of the resonance and the separation among the different observed resonances, in terms of the displacement Δz, was obtained by moving monotonically the conducting ring near one of the plane surfaces of the resonator. The related values in terms of frequency were calculated by means of a calibration obtained from the value calculated for the free spectral range.

In what concerns point 3), these measurements allow to verify the effectiveness of the approximate expressions (16) and (17) of the fields. Here the coupling circuit is kept in fixed condition corresponding to the best matching; the tuning ring is also, for each complete series of measurements, in a fixed position at the maximum of the resonance. The dielectric antenna connected to a detector is moved by a micrometer drive along the different directions of interest. The movement along the radius of the disc allows to determine the modal index m; the study of field intensity along the axis of the disc gives in turn the modal index l.

V. Results and Discussion

A general picture of the mode distribution of the dielectric disc used as a WGM resonator is given in Fig. 5. In this case, the polarizer is eliminated from the transmission line in order to have elliptical polarization that enables the excitation of all modes. In addition, the position p of the antenna along the radius and the distance z of the tuning metallic ring from the plane surface of the disc are simultaneously varied. It turns out a three-dimensional graph showing in one dimension the variation of the wave intensity in the space domain and in the other dimension the variation of the wave intensity in the tuning domain. The distribution of modes in the resonator also remains the same as that shown in Fig. 5 when the dimension of the excitation guide or its position with respect to the rim of the resonator are changed in the coupling scheme; consequently, it is argued that the spectrum represented in Fig. 5 is just the spectrum of the resonator in the presence of the tuning device. The analysis of different modes by means of polarized radiation gave more detailed results, allowing, for instance, to find out that the resonance labeled 1 in Fig. 5 is given by the overlap of two nearly degenerate modes, the one WGE (mode 1a) and the other WGH (mode 1b).

The measure of the effectiveness of the coupling between guide and resonator was obtained by changing monotonically the distance $\boldsymbol{s}$ between the excitation guide and the resonator as well the position of the tuning device with respect to the resonator surface. Fig. 6(a) shows the contour plot representation of the transmission signal in the case of mode 1a. The shift of the maximum of the resonance in the tuning domain is evident when $\boldsymbol{s}$ is changed; this effect is due to the variation of the resonance frequency of the resonator caused by the presence of the dielectric waveguide. The simultaneous observation of the reaction signal gives exactly the same results, even if with an inverse trend. It must be noticed that the reaction signal in the best matching condition vanishes, indicating that the condition of the critical coupling is reached. Fig. 6(b) shows the contour plot of the transmission signal for mode 1b. Here the resonance frequency is subjected to a shift having the same sign as in the previous one; in Fig. 6(a) and (b) the trend seems opposite, but this occurs since the tuning effect of the conductor ring (19a) has opposite value for the WGE and WGH modes [15].

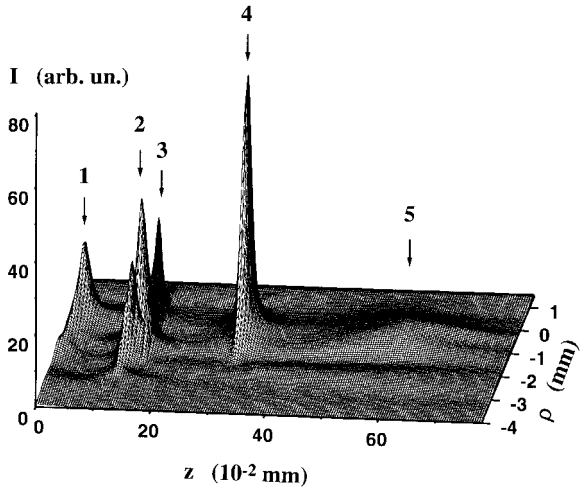

Fig. 5. Overall representation of resonant modes observed with unpolarized radiation in the dielectric resonator; z represents the distance of the tuning ring from the resonator plane surface and ρ the position along the resonator radius; $\rho = 0$ indicates the rim of the resonator.

The measurement of merit factor Q and of free spectral range for the different mode families were obtained by exploiting (19b). By assuming A and B constant for modes with consecutive values of n ($n \gg 1$), the fit of the position of at least three modes of resonance using (19b) gives the calibration of the tuning effect in terms of the displacement Δz of the tuning ring. The measurements were carried out with two resonators having the same dimensions but made with polyethylene material having different molecular weights. Fig. 7 shows the position of the resonances for five modes $\mathrm{WGH}_{n,0,0}$ measured in terms of Δz. The related frequency variations are reported in units of free spectral range. The continuous curve represents the fit of the experimental values with (19b). The agreement is very good and confirms the effectiveness of involved approximations.

The measured Q (*finesse*) range is between 1500 and 3000 ($\approx 15 \div 30$) for the resonator #1 and between 300 and 1900 ($\approx 3 \div 19$) for the resonator #2. The experimental results suggest that the polyethylene material forming the resonator #1 has fewer losses than that of the resonator #2; furthermore, the modes with the index $m = 0$ show Q values greater than the ones for the corresponding modes with $m = 1$ that have a larger irradiated power. The tuning device, in addition, does not affect significantly the Q-factor of the resonator, as argued from the not regular trend of Q-factors observed for the different WGH modes. Finally, WGH modes show values of Q higher than the corresponding WGE. This is due probably to the fact that in the case of WGE modes a good coupling is obtained with positions of the dielectric guide closer to the resonator than in the case of WGH modes.

The determination of the spatial distribution of field intensity was made by moving the pickup antenna for each resonance on the plane surface of the resonator along the radius and on the lateral surface along the axial direction. Fig. 8(a) shows the results of experiments (dots) for mode 4 of Fig. 5.

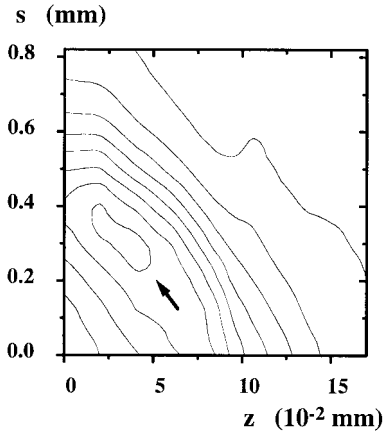

(a)

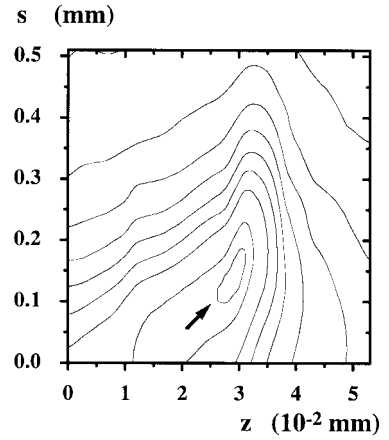

(b)

Fig. 6. Contour plots of the transmission resonance signal of mode 1 of Fig. 5, obtained with the experimental scheme shown in Fig. 4b; s represents the distance between the waveguide and the resonator. (a) Mode 1a (WGE) of Fig. 5; (b) mode 1b (WGH) of Fig. 5. The arrows indicate the contour lines of the maximum of the signal.

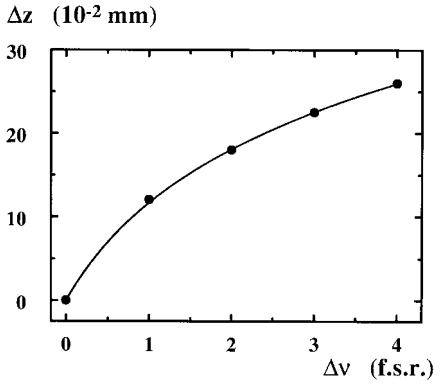

Fig. 7. Measurements of the displacement Δz for contiguous $\mathrm{WGH}_{n,0,0}$ resonances. The origin of the coordinate Δz is arbitrarily fixed at a resonance. The solid line represents the fit of the experimental data with (19b).

Such results can be compared with the values of the energy flux in the direction of interest for the WGM's with weak axial propagation. By sensing the energy along the radius of the resonator surface with the antenna perpendicular to the radius, the flux of energy to be considered corresponds to the azimuthal component of the Poynting vector $\langle S_\varphi \rangle$ calculated starting from (16) and (17) for the different field components.

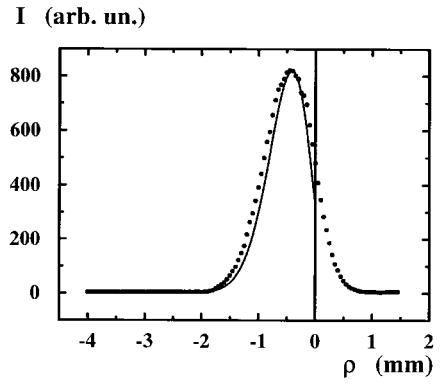

(a)

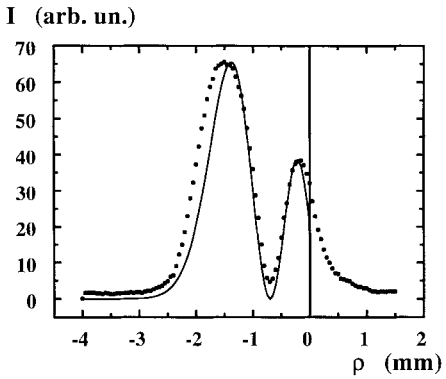

(b)

Fig. 8. Measurements (dots) of the radial distribution of the field intensity for two different WGH resonant modes with different modal index m; (a) mode 4 of Fig. 5, $m = 0$; (b) mode 2 of Fig. 5, $m = 1$. The vertical lines indicate the position of the rim of the resonator; the values calculated fitting the experimental data with (20) are also reported (solid line).

The expression of such component for both of the modes WGE and WGH with azimuthal mode index n is

$$\langle S_\varphi \rangle \propto \frac{J_n^2(k_1\rho)}{\rho}. \tag{20}$$

The determination of the index n can be performed with different methods. A simple method that allows to attribute the value n consists of comparing the experimental curve with calculated curves corresponding to the expression (20) with different values of n. The solid curve reported in Fig. 8(a) corresponds to the value $n = 103$; the observed trend indicates that this mode has the modal index $m = 0$. Fig. 8(b) (dots) reports the results for mode 2 of Fig. 5; the trend gives evidence that this mode has the index $m = 1$. The theoretical values (solid line) reported in this case are calculated by putting in (20) the index $n = 96$.

The field distribution in axial direction is obtained by sensing the intensity at the rim of the resonator by the same antenna. Fig. 9 reports (dots) the trend of the field intensity for mode 3 (Fig. 5) measured as a function of the coordinate ζ where the zero was fixed at the plane of symmetry perpendicular to the axis of the resonator. The vertical dotted lines indicate the positions of the plane surfaces of the resonator. A qualitative interpretation of the observed trend both inside and outside the resonator is obtained by resorting to the fundamental symmetric solution already mentioned in Section

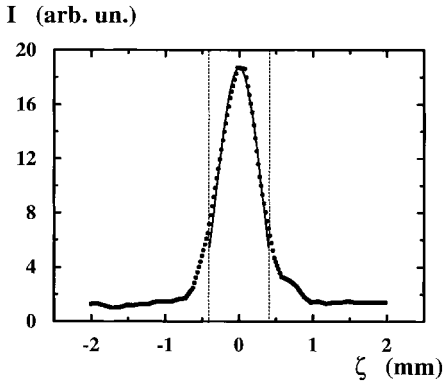

Fig. 9. Measurements (dots) of the axial distribution of the field intensity of the resonance of Fig. (5); $\zeta = 0$ corresponds to the equatorial plane of the resonator. The vertical lines indicate the position of the plane surfaces. The solid line fits the experimental data with a function proportional to $(\cos\{hz\})^2$.

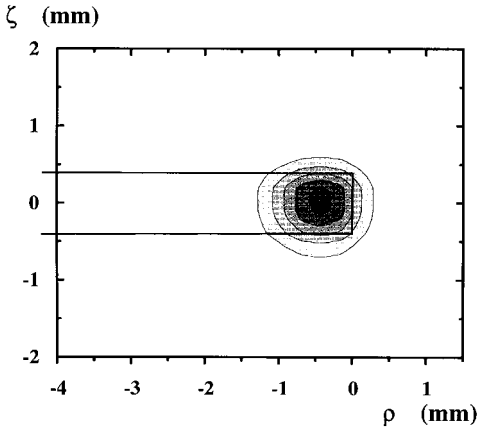

Fig. 10. Contour line representation of the field intensity of the resonant mode 4 of Fig. (5) in an axial section of the resonator. The difference between two contiguous curves is constant; the darkest zone corresponds to the maximum intensity. The solid line represents the section of the resonator near the rim.

II:

$$\psi(\zeta) = A\cos(h\zeta) \quad |\zeta| < \frac{w}{2}; \quad \psi(\zeta) = Be^{-h'|\zeta|} \quad |\zeta| > \frac{w}{2} \tag{21}$$

where w is the thickness of the resonator [21]. The propagation constants h and h' can be connected each other by the relation [27]

$$\begin{aligned} h' &= \omega\sqrt{\varepsilon_2\mu_0}\sqrt{(\sin(\Theta_i))^2\left(\frac{\varepsilon_1}{\varepsilon_2}\right) - 1} \\ &= \omega\sqrt{\varepsilon_2\mu_0}\sqrt{\left(1 - \frac{h^2}{k_1^2}\right)\left(\frac{\varepsilon_1}{\varepsilon_2}\right) - 1}. \end{aligned} \tag{22}$$

Equation (22) combined with the conditions of continuity and continuous first derivative at $\zeta = w/2$ [14] becomes

$$h\tan\left(h\frac{w}{2}\right) = h' = \omega\sqrt{\varepsilon_2\mu_0}\sqrt{\left(1 - \frac{h^2}{k_1^2}\right)\left(\frac{\varepsilon_1}{\varepsilon_2}\right) - 1}. \tag{23}$$

For the resonators employed, (23) gives the value $h \approx 2.5$ mm^{-1}. The continuous line in Fig. 9 is the fit of experimental data with the function $(\cos\{h\zeta\})^2$; the fairly good agreement enforces the effectiveness of the theoretical picture and evidences the directivity of the antenna.

The measurement of the pattern of field intensity can be carried out only at the surfaces of the resonator; the bulk field arrangement can be reasonably inferred by assuming that the radial distribution is constant along the dimension ζ. Analogously, the field distribution along the axis must be independent of the position along the radius considered. Fig. 10 shows the resonator with the field distribution obtained for mode 4 of Fig. 5 described by a contour plot representation. It must be pointed out that the reported pattern qualitatively resembles the ones reported in [11], calculated numerically for configurations like that here considered.

VI. Conclusions

The work here presented deals with the different problems relevant to the dielectric resonators working with the whispering gallery modes. Starting from the fundamentals of the propagation of electromagnetic waves in cylindrical structures, the whispering gallery modes are characterized; particular attention is focused on the low-loss modes with weak axial propagation constant and a deeper insight is given to the role of the total reflection at the cylindrical surface in the different regimes. The propagation of modes is interpreted in terms of expansion with plane waves propagating at different angles with respect to the axis of the cylinder; the low-loss modes correspond to the plane waves incident on the cylindrical surface at angles greater than the limit angle. For a cylindrical resonator with finite axial dimension, the low-loss resonances occur when the total reflection condition is fulfilled at both the curved lateral surface and the plane circular surfaces. The approximate analytical expressions of fields are obtained for both nearly transverse electrical (WGE) and transverse magnetic (WGH) modes by a proper expansion in terms of the longitudinal components calculated from a characteristic equation.

The problem of the coupling of the radiation from a transmission line to the resonator operating with WGM's is carefully examined. This problem is faced by investigating the conditions that give the same phase velocity in the two structures—the phase velocity in a circular cylindrical dielectric guide changes continuously with the diameter of the cylinder. The coupling of radiation to the resonator is then obtained by using a tapered waveguide. The evanescent field near the waveguide can be described by resorting again to the model of expansion of modes in plane waves; in this case, the evanescent field also arises from the total reflection mechanism occurring when the waves are propagating with incidence angles greater than the limit angle. In all of the cases, the impact of different approximations is deeply discussed and properly taken into account.

The system transmission line WG resonator was tested at 240 GHz. A proper experimental scheme was used to tune the resonator across the different resonances. The fields at the surface of the resonator were picked up by a dielectric antenna movable in a controlled way. A detailed characterization of the coupling method was possible and several resonances were classified and analyzed. The experimental analysis of the field distribution was performed on different resonance

modes and the comparison with theoretical predictions was very satisfactory.

In conclusion, a method is suggested to calculate in an analytical way the approximate expressions for the fields in whispering gallery modes of a disc-shaped dielectric resonator. The experimental methodologies used to characterize these devices at hundreds of gigahertz are based on the theoretical analysis of the different effects involved, and the results show a remarkable agreement with the predictions.

REFERENCES

[1] X. H. Jiao, P. Guillon, L. A. Bermudez, and P. Auxemery, "Whispering-gallery modes of dielectric structures: Applications to millimeter-wave bandstop filters," *IEEE Trans. Microwave Theory Tech.*, vol. MTT-35, pp. 1169–1175, Dec. 1987.

[2] X. H. Jiao, P. Guillon, P. Auxemery, and D. Cros, "Dielectric resonators for use in planar integrated circuits at short millimeter wavelengths," *IEEE Trans. Microwave Theory Tech.*, vol. 37, pp. 432–437, Feb. 1989.

[3] X. H. Jiao, P. Guillon, and J. Obregon, "Theoretical analysis of the coupling between whispering-gallery dielectric resonator modes and transmission lines," *Electron. Lett.*, vol. 21, no. 3, pp. 88–89, 1985.

[4] M. Muraguchi, K. Araki, and Y. Naito, "A new type of isolator for millimeter-wave integrated circuits using a nonreciprocal travelling-wave resonator," *IEEE Trans. Microwave Theory Tech.*, vol. MTT-30, pp. 1867–1873, Nov. 1982.

[5] D. Cros and P. Guillon, "Whispering gallery dielectric resonator modes for W-band devices," *IEEE Trans. Microwave Theory Tech.*, vol. 38, pp. 1667–1674, Nov. 1990.

[6] I. Longo, "An investigation of the travelling wave dielectric resonator for the applications to electron spin resonance experiments," *Meas. Sci. Technol.*, vol. 2, pp. 1169–1176, 1991.

[7] J. Krupka, "Resonant modes in shielded cylindrical ferrite and single-crystal dielectric resonators," *IEEE Trans. Microwave Theory Tech.*, vol. 37, pp. 691–697, Apr. 1989.

[8] I. Longo, "Atomic and molecular spectroscopy in the evanescent electromagnetic field of dielectric resonators," *Int. J. Infrared Millim. Waves*, vol. 14, pp. 601–616, 1993.

[9] D. G. Blair, E. N. Ivanov, and H. Peng, "Sapphire dielectric resonator transducer," *J. Phys. D, Appl. Phys.*, vol. 25, pp. 1110–1115, 1992.

[10] A. Colligiani, I. Longo, M. Martinelli, M. Lucchesi, and L. Pardi, "A wide-band whispering gallery mode dielectric resonator having multiple high-Q cavities for high field ESR spectroscopy," *Appl. Magn. Reson.*, vol. 9, pp. 567–579, 1995.

[11] J. Krupka, D. Cros, M. Aubourg, and P. Guillon, "Study of whispering gallery modes in anisotropic single-crystal dielectric resonators," *IEEE Trans. Microwave Theory Tech.*, vol. 42, pp. 56–61, Jan. 1994.

[12] D. E. Budil, K. A. Earle, W. B. Lynch, and J. H. Freed, "Electron paramagnetic resonance at 1 millimeter wavelengths," in *Advanced EPR, Applications in Biology and Biochemistry*, A. J. Hoff, Ed. Amsterdam, The netherlands: Elsevier, 1989.

[13] D. Kajfez and P. Guillon, *Dielectric Resonators.* Norwood, MA: Artech House, 1986.

[14] C. Vedrenne and J. Arnaud, "Whispering-gallery modes of dielectric resonators," *Proc. Inst. Elect. Eng.*, vol. 129, pt. H, no. 4, pp. 183–187, 1982.

[15] D. Cros, "Les 'whispering gallery' modes des resonateurs dielectriques: application aux oscillateurs et combineurs de puissance millimetriques," These de Doctorat, Université de Limoges, France, 1990.

[16] A. Yu. Bresgunov, A. A. Dubinskii, V. N. Krimov, O. G. Poluektov, and Ya. S. Lebedev, "Pulsed EPR in 2-mm band," *Appl. Magn. Reson.*, vol. 2, pp. 715–728, 1991.

[17] F. Strumia and M. Inguscio, "Stark spectroscopy and frequency tuning," in *Infrared and Millimeter Waves*, vol. 5, K. J. Button, Ed. New York: Academic, 1982.

[18] C. P. Poole Jr., *Electron Spin Resonance.* New York: Wiley-Interscience, 1982.

[19] E. A. J. Marcatili and R. A. Schmeltzer, "Hollow metallic and dielectric waveguides for long distance optical transmission and lasers," *Bell Syst. Tech. J.*, vol. 43, pp. 1783–1809, 1964.

[20] J. A. Stratton, *Electromagnetic Theory*. New York: McGraw-Hill, 1941.

[21] N. S. Kapany and J. J. Burke, *Optical Waveguides.* New York: Academic, 1972.

[22] R. A. Waldron, *Theory of Guided Electromagnetic Waves*. London, U.K.: Van Nostrand, 1969.

[23] L. V. Weinstein, *Open Resonators and Open Waveguides*. Boulder, CO: Golem, 1969.

[24] Lord Rayleigh, "The problem of whispering gallery," *Phil. Mag.*, vol. 20, pp. 1001–1004, 1910.

[25] C. C. Johnson, *Field and Wave Electrodynamics*. New York: McGraw-Hill, 1965.

[26] D. G. Kiely, *Dielectric Aerials*. London U.K.: Methuen, 1953.

[27] M. Born and E. Wolf, *Principles of Optics*. London U.K.: Pergamon, 1959.

Giuseppe Annino was born in Gallipoli, Italy, in 1967. He received the M.S. degree with honors from the University of Pisa, Italy, in 1996, with a dissertation on the application of whispering gallery resonators in high-field electron paramagnetic resonance spectroscopy.

He is now with Scuola Normale Superiore in Pisa, Italy, where he is investigating the properties of semiconductor heterostructures in a high magnetic field.

Mario Cassettari received the M.S. degree in physics from the University of Pisa, Italy, in 1967.

He is presently a Senior Researcher at the Institute for Atomic and Molecular Physics of the Italian National Research Council, Pisa, Italy. His scientific interests are mainly in phenomena occurring in phase transitions of the first and second order, and in relevant properties of hydrogen-bonded liquids and polymeric materials, studied from both experimental and theoretical points of view. His experimental activity has been devoted chiefly to the study of thermodynamic and dielectric properties of the investigated systems, and his current research on millimetric waves is focused on dielectric studies in the THz region.

Dr. Cassettari is a member of the Italian Physical Society.

Iginio Longo received the M.S. degree in physics from the University of Pisa, Italy, in 1968.

Since 1970, he has been with the Institute for Atomic and Molecular Physics of the National Research Council (CNR), Pisa, Italy, where he is currently a Senior Scientist. He has performed research in atomic and molecular spectroscopy and quantum electronics. Currently, he is involved in the study of dielectric waveguides and resonators at millimeter and FIR wavelengths and their applications to new spectroscopic techniques.

Massimo Martinelli received the M.S. degree in physics from the University of Pisa, Italy, in 1969.

From 1969 until 1992, he was with the Institute of Physics, University of Pisa, Italy. In 1992 he joined in the staff of the Institute for Atomic and Molecular Physics of the National Research Council, Pisa, Italy, as a Research Director. Since 1994 he has been the Director of the Institute. His research activity has been devoted to the study of new methodologies of linear and nonlinear magnetic resonance spectroscopies, microwave spectroscopies, dielectric characterization of materials, and nonlinear behavior of complex systems. He is currently coordinating research of a new high-field electron paramagnetic resonance apparatus involving the use of whispering gallery resonators at submillimeter wavelengths.

Mr. Martinelli is a member of the International AMPERE Committee.